Synthesis of cubic zirconium(IV) nitride, c-Zr3N4, in the 6–8 GPa pressure region

Takashi Taniguchi, Dmytro Dzivenko, Ralf Riedel, Thierry Chauveau, Andreas Zerr

Synthesis of cubic zirconium(IV) nitride, c-Zr_3N_4, in the 6-8 GPa pressure region

Takashi Taniguchi[a,*], Dmytro Dzivenko[b,†], Ralf Riedel[b], Thierry Chauveau[c], Andreas Zerr[c*]

[a] *National Institute for Materials Science, Tsukuba Ibaraki 305-0044, Japan*

[b] *FB Material- und Geowissenschaften, Technische Universität Darmstadt, 64287 Darmstadt, Germany*

[c] *LSPM, CNRS-UPR 3407, Université Paris 13, 93430 Villetaneuse, France*

We report on the lowermost pressure and temperature conditions where cubic zirconium(IV) nitride having Th_3P_4-type structure, c-Zr_3N_4, forms in a belt-type apparatus. This novel hard material having exceptional wear resistance by machining of low-carbon steels appears at pressures between 6.5 and 7.7 GPa when heated to 1400-1600 ^{o}C. Single-phase samples were obtained at P=7.7 GPa thus indicating that the industrial scale synthesis of this innovative material is feasible. Chemical reaction of the sample material with the Pt-capsule led to formation of a Pt-Zr alloy, as a minor admixture, which can potentially be used as a binder for cementing of polycrystalline c-Zr_3N_4 tools.

Keywords: D. Nitrides; A. Powders: solid state reaction; A. Hot pressing; B. X-ray methods; High-pressure high-temperature synthesis; hard materials

---

* Corresponding authors.
E-mail addresses: zerr@univ-paris13.fr (A. Zerr); taniguchi.takashi@nims.go.jp (T. Taniguchi)
† now with NAGEL Maschinen- u. Werkzeugfabrik GmbH, 72622 Nürtingen, Germany

1. Introduction

Zirconium(IV) nitride having cubic Th_3P_4–type structure, c-Zr_3N_4, is a novel hard, stiff and highly wear resistant ceramic material which is thermodynamically stable at high pressures and high temperatures (HP-HT) [1] as is the case for diamond, the hardest known material. The hardness of dense c-Zr_3N_4 coatings, measured using nano-indentation method, was found to be 36-37 GPa [2]. The bulk and shear moduli of the densified polycrystalline c-Zr_3N_4 were determined, after evaluation of the porosity influence, to be B_0=217(20) GPa and G_0=163(9) GPa, respectively [3]. These values are lower than those of diamond or cubic BN (c-BN) but the potential of c-Zr_3N_4 as an industrial material relies on its outstanding wear resistance by milling of low carbon steels. The latter followed from investigation of c-Zr_3N_4 coatings obtained via a modified filtered cathodic arc (FCA) method which showed wear resistance ~10 times higher than that of TiN coatings and much higher than that of cubic BN in tribological contact with steels [2, 4, 5].

Macroscopic bodies of c-Zr_3N_4 (~10 mg in weight and ~1 mm in size) were earlier obtained via HP-HT syntheses at P=12 GPa and t=1600 ^{o}C [6] using nanocrystalline n-Zr_3N_{4+x} having distorted NaCl structure [7] as a starting material. However, the lowest pressure of formation of c-Zr_3N_4 was not determined experimentally prior our work. According to the theoretical predictions, c-Zr_3N_4 should form at much lower pressures of 6 GPa but decompose to the mono-nitride ZrN if heated slightly above the room temperature [8]. The prediction appeared to be not consistent with the above mentioned thermodynamic stability of c-Zr_3N_4 at 12 GPa and 1600 ^{o}C. Thus, an experimental realization of the P-T phase diagram of the zirconium(IV) nitride at pressures between 5 and 8 GPa and its stability with respect to decomposition to ZrN were necessary. This pressure region is of outstanding importance because it includes the region where the industrial scale synthesis can be carried out using belt-type HP-HT apparatuses providing large samples suitable for standardized tests. Such tests are necessary to ascertain the industrial applicability of c-Zr_3N_4.

The purpose of our work was therefore to clarify the lowermost *P*-*T* conditions of synthesis of c-Zr_3N_4 by using a belt-type HP-HT apparatus. In addition, examination of the recovered products led us to a method potentially suitable for cementing of polycrystalline c-Zr_3N_4 using a metallic binder, similar to the well-known industrial approach developed for the cemented tungsten carbide e.g. [9].

2. Materials and methods

As in the previous work, nanocrystalline *n*-Zr_3N_{4+x} was used as the starting material. It was obtained in form of granulated powder in large amounts via ammonolysis of tetrakis-(diethylamido)-zirconium ($Zr(NEt_2)_4$) at 600 ºC [7] which provides reproducibly an overstoichiometric composition with x>0 (Table 1). The content of nitrogen was determined using the hot-gas extraction (HGE) method described below. The HGE measurements showed also minor amounts of carbon of 1.4(1) wt% and of oxygen of 0.6(1) wt% in the starting *n*-Zr_3N_{4+x} (Table 1). The main mechanism of carbon incorporation in the ammonolysis product is, according to the original work [7], intramolecular β-hydrogen activation leading to formation of metallocycles, M-N-C rings with strong M-C bonds. Decomposition of the Et-groups in

$Zr(NEt_2)_4$ into free carbon, before they were removed via the ammonolysis, was considered as the secondary mechanism [7]. The oxygen contamination is a result of accumulation of traces of H_2O and O_2 adsorbed on the walls of the glass ware and the gas supplying lines used for the synthesis of ($Zr(NEt_2)_4$) from $ZrCl_4$, diethylamine, and butyl-lithium as well as during the subsequent ammonolysis [7]. Fig.1 shows an X-ray diffraction (XRD) pattern and an SEM image of the starting n-Zr_3N_{4+x} granules (agglomerates of nanocrystals) of nearly 100 nm in size. Availability of this starting material makes possible the synthesis of c-Zr_3N_4 in large volume HP-HT apparatuses which do not permit loading of condensed nitrogen in the reaction volume needed to perform a nitridation reaction of the type $3 \cdot ZrN + 0.5 \cdot N_2 \rightarrow$ c-Zr_3N_4 *in-situ* at high pressures.

Belt-type HP-HT apparatuses of standard design [10] allow for achieving pressures and temperatures to 6 GPa and 1600 ºC, respectively, where diamond and cubic BN can be synthesized in volumes approaching 500 cm^3 [11, 12]. Thanks to recent developments, temperatures to 2100 ºC and pressures to 10 GPa became routinely accessible in modified belt-type apparatuses one of which we used here [13, 14]. The maximal sample size in our apparatus was 10 mm in diameter and 6 mm in height. We used an assembly containing two samples of 7 mm in diameter and 3 mm in height (Fig.2) in order to examine different capsule materials, namely platinum and tantalum. The HP-HT synthesis was performed via a compression of the starting material to a desired pressure at room temperature, heating to a chosen temperature during 20 min, holding at that temperature for 20 min, and quenching.

Phase composition of the recovered products was determined from XRD patterns obtained using two diffractometers. The first one (Inel four circle diffractometer, long-line fine focus Copper X-ray source, flat Ge (111) monochromator, $\lambda(\text{Cu-K}_{\alpha1})$=1.54056 Å, curved position-sensitive detector CPS 590) was used for the phase identification because it provided a high angular resolution $\delta 2\theta$=0.02°-0.08°, depending on the diffraction angle. XRD patterns suitable for the structure refinement and quantitative phase analysis were collected in the Debye-Scherrer geometry using a STOE STADI P diffractometer (Stoe & Cie GmbH, Molybdenum X-ray source, a flat Ge (111) monochromator, $\lambda(\text{Mo-K}_{\alpha1})$=0.70932 Å) equipped with a linear position sensitive detector covering the 2θ region of 6°. The sample powder in a glass capillary of 0.3 mm in diameter defined the angular resolution of the system to be $\delta 2\theta$=0.1°.

In order to determine chemical composition of the recovered products, as well as of the starting n-Zr_3N_{4+x}, we measured contents of nitrogen, oxygen, and carbon using the hot-gas extraction (HGE) method and metals were assumed to count for the rest. Precision of the LECO TC-436- and LECO C-200 analyzers (LECO Corporation) suitable for the nitrogen/oxygen and carbon analysis, respectively, was 0.5% RSD.

We also measured Raman spectra of the products which were excited by an Ar-ion laser (λ= 514.5 nm) and recorded using a LabRam HR800 spectrometer (Horiba Jobin Yvon). A scanning electron microscope (HR-SEM, Philips XL30 FEG) was applied to analyse texture of the products and grain morphology.

3. Results and Discussion

XRD patterns of the samples synthesized at P=7.7 GPa (Fig.3) showed that at 1500-1600 ºC the starting n-Zr_3N_{4+x} transformed to c-Zr_3N_4 only. At higher temperature, near t=1800 ºC, traces of ZrN appeared and after heating to t=2050 ºC only the mono-nitride was recovered indicating release of nitrogen at that high temperature. These findings are summarized, together with the synthesis results at other P-T conditions, in a P-T diagram shown in Figure 4.

The lowest pressure where c-Zr_3N_4 appeared was found to be 6.5 GPa while heated to t=1400-1600 ºC (Fig.4). However, the product was contaminated by another not yet reported Zr-N phase appearing to have, according to our preliminary analysis, either monoclinic or triclinic structure. A detailed characterization of this novel Zr-N phase, denoted hereafter as ls-Zr_xN_y, is the subject of a future work. At the same pressure but higher temperatures, the mono-nitride ZrN formed. In Fig.4 we also show, qualitatively, relative contents of the Zr-N compounds/phases formed at each of the chosen P-T conditions, derived from the measured XRD patterns.

In order to verify the chemical and phase purity of the products obtained at P = 7.7 GPa and t = 1500-1600 ºC, a detailed characterization was performed using XRD, elemental analysis, scanning electron microscopy and Raman spectroscopy. XRD patterns (Fig. 5) of a sample synthesised in a platinum capsule (sample s5424) led us to a method potentially suitable for densification of polycrystalline bodies of c-Zr_3N_4. They showed, in addition to peaks of c-Zr_3N_4, weak peaks belonging to two other compounds: One of them was a Pt-Zr alloy having cubic lattice parameter a_0=3.9885(3) Å. This product of a reaction of the platinum capsule with our sample material could be either a solid solution of Zr in the fcc-lattice of elemental platinum, $Pt_{1-x}Zr_x$, or an intermetallic binary compound Pt_4Zr having an $AuCu_3$ related structure [15, 16]. We could not give preference to any of these phases because all observed XRD peaks can be described by an fcc-lattice but with the cubic parameter significantly larger than that reported for $Pt_{1-x}Zr_x$ [15, 17]. On the other hand, our experimental cubic lattice parameter is similar to that of Pt_4Zr but the (100)-peak of this compound at 2θ=10.20° was not visible in the XRD patterns even though it could not be obscured by any other peaks in the vicinity (Fig. 5). A possible explanation of the inconsistency could be presence of nitrogen in the lattice of the Pt-Zr alloy. Our XRD patterns did not permit to examine this possibility in more detail due to a small amount of the by-product and, accordingly, low intensities of the related diffraction peaks. If it indeed contained nitrogen then it would closely resemble the cubic solid solution of tungsten carbide in cobalt β-Co(WC) serving as the binder in cemented carbides of tungsten [9]: Independent of the structure and composition, such Pt-Zr or Pt-Zr-N alloy could play the same role by cementing of polycrystalline c-Zr_3N_4 bodies. According to our Rietveld refinement, the alloy made ~0.5% of the whole sample weight (Table 1).

A Zr-O rich compound having fluorite-related structure was recognized as the second minor admixture which amount was below 4 wt% of the whole sample material (Table 1). This could be either ZrO_2 having ideal cubic structure (c-ZrO_2) with the lattice parameter a_0=5.0970(7) Å, possibly stabilized by nitrogen, or β-$Zr_7O_8N_4$ having rhombohedral fluorite-related lattice with ordered anion vacancies [18, 19]. Both compounds are known to appear, at atmospheric pressure, on the N-rich side of the ZrO_2-Zr_3N_4 system [20]. Since they have the same intense XRD peaks and the admixture amount was small, we could not give preference to any of the solutions. However, all found peaks could be attributed to c-ZrO_2 with the lattice parameter a_0=5.0970(7) Å which diffraction pattern is less complex than that of β-$Zr_7O_8N_4$. According to the literature, binary c-ZrO_2 is quenchable to ambient conditions only if it is nanocrystalline or nonstoichiometric [21, 22]. On the other hand, recovery of N-stabilized c-ZrO_2 to ambient conditions was claimed in some earlier reports [23-25].

Results of the HGE-analysis of the sample synthesized in the Pt-capsule at $P = 7.7$ GPa and $t = 1500$ °C indicated a moderate decrease of the average nitrogen content to 16.6(5) wt% when compared with that of the starting over-stoichiometric *n*-Zr_3N_{4+x} (Table 1). This value agrees, however, whit that expected for the stoichiometric Zr_3N_4, namely 17 wt%, if the experimental uncertainty is taken into account. A minor increase of the oxygen content to 1.4 wt% confirms the earlier observed slow diffusion of oxygen from the surrounding pressure medium containing oxydes, e.g. ZrO_2 in our case (Figure 2), through the Pt capsule into the sample volume at the *P-T* conditions of the synthesis [6]. In contrast, the carbon content of 1.6(1) wt% remained unchanged. Raman spectra and SEM images of the product (Fig. 6) suggested that carbon was not incorporated in any of the crystalline phases but precipitated as disordered graphite in form of thin platelets. The latter was concluded from observation of three broad peaks at 1365 cm^{-1}, 1587 cm^{-1}, and 1626 cm^{-1} corresponding to the D-, G-, and D´ bands of disordered graphite [26]. No Raman peaks belonging to any of the above mentioned Zr-O-N phases were recognized, most probably because they exhibit broad and weak peaks only [27, 28].

Presence of the Pt-Zr based alloy and of the Zr-O rich phase as well as a high contrast in the X-ray scattering power of the constituting elements (Zr and Pt on the one hand; N and O on the other) did not permit determining the degree of substitution of nitrogen by oxygen on the anion sites of c-Zr_3N_4 from the Rietveld refinement. As earlier reported, such substitution leads to formation of an oxygen bearing zirconium(IV) nitride c-$Zr_{3-u}(N_{1-u},O_u)_4$ with the u-value up to 0.12 [6]. For our sample, the Rietveld refinement and the HGE measurements would agree for $u \leq 0.02$.

XRD patterns of the product synthesized in a Ta-capsule at $P = 7.7$ GPa and $t = 1500$ ºC (sample s5006) showed, in addition to the main product having cubic Th_3P_4-type structure with the lattice parameter a_0=6.7550(1) Å, the presence of three minor by-products: A Zr-O rich compound having a fluorite related structure which could be attributed to c-ZrO_2 with a_0 = 5.0920(6) Å, a suboxide Ta_2O [29] and a subnitride $TaN_{0.5}$ [30]. Preliminary analysis of the XRD patterns suggested that the amount of c-ZrO_2 could not exceed 5 wt% and the total amount of the binary Ta-compounds was below 2 wt%. Absence of peaks which could be attributed to a Ta-Zr alloy suggested that Ta is not suitable for densification of polycrystalline c-Zr_3N_4 bodies. As above, Raman spectra revealed the presence of disordered graphite in the sample. The SEM images showed crystals of the main product of ~400 nm in size and thin platelets which we attributed to disordered graphite.

The HGE analysis of the sample showed significantly lower contents of all three light elements when compared with the product synthesized in a Pt capsule at the same *P*-*T* conditions (Table 1). However, the content of oxygen was still above that of the starting material. This intermediate content of oxygen could be explained by a smaller amount of oxygen diffused inside the Ta-capsule because it was protected by graphite discs above and below (Figure 2) which served as oxygen traps. The lower carbon content, when compared with that of the starting material, could be caused by the reaction with the Ta-capsule leading to the formation of TaC. This could be concluded from the gold-brown colour of the inner walls of the Ta-capsule recognised after the sample recovery. Similarly, a competing reaction of oxygen with the Ta-capsule could lead to formation of Ta_2O on the capsule walls and thus cause the lower oxygen content in the sample when compared with that in the product synthesized in a Pt capsule. However, incorporation of a significant amount of heavy Ta atoms in the structure of the main HP-HT product leading to the formation of the ternary c-$(Zr_{1-x}Ta_x)_3N_4$ would better explain the lower contents of the light elements in the HGE measurements, especially of nitrogen. This is because few wt% of Ta_2O and $TaN_{0.5}$, recognised in the XRD patterns, couldn't compensate the difference in the amount of the light element even if the anomalous absorption of X-rays by tantalum atoms is taken into account. The latter could artificially reduce amount of the Ta-containing phases, as derived from the XRD patterns, but not significantly. Assuming the formation of c-$(Zr_{1-x}Ta_x)_3N_4$, we succeeded to establish a reasonable agreement of the HGE-data with the Rietveld refinement for the following phase composition of the product (Table 1): 93.9(3) wt% of c-$(Zr_{0.84}Ta_{0.16})_3N_4$, 3.5(1) wt% of c-$ZrO_2$, 1.2(1) wt% of Ta_2O and 0.3(1) wt% of $TaN_{0.5}$. Here, the presence of 1.1 wt% of carbon was already taken into account. From this Rietveld refinement, the total N- and O-contents were calculated to be 14.3(1) wt% and 1.0(1) wt%, respectively, which are close to the HGE values (Table 1). It should be emphasized that the proposed formation of the ternary c-$(Zr_{1-x}Ta_x)_3N_4$ needs further verification. Large grains of a few μm in size (well above those in the present work) or single phase samples are needed to confirm existence of this ternary compound using, for example, the electron probe microanalysis (EPMA). This technique, permitting reliable quantitative chemical analysis of such materials, was successfully applied in our earlier studies on dense transition metal nitrides [6, 31].

4. Conclusion

The main result of our work is the formation of c-Zr_3N_4 in a belt-type apparatus at pressures between 6.5 and 7.7 GPa which makes the industrial scale synthesis of this material in form of bulk objects suitable for standardized tests feasible. At P=7.7 GPa, nearly single phase samples of c-Zr_3N_4 (at least 95% of the weight) were obtained. Another observation, important for practical applications, is the formation of a Pt-Zr based alloy via the reaction of platinum with the sample material. Similarly to the well known method of cementing of tungsten carbide by cobalt e.g. [9], this alloy could serve as a binder by fabrication of dense polycrystalline c-Zr_3N_4 bodies. Finally, we maybe have succeeded to quench c-ZrO_2 to ambient conditions. If this is the case then the phase was stabilized by nitrogen.

Acknowledgements

The authors thank N. Nicoloso for fruitful discussions during preparation of the manuscript. T.T. acknowledges support from the Elemental Strategy Initiative conducted by the MEXT, Japan.

REFERENCES

[1] A. Zerr, G. Miehe, R. Riedel, Synthesis of cubic zirconium and hafnium nitride having Th_3P_4-structure, Nat. Mater. 2 (2003) 185-189.

[2] M. Chhowalla, H.E. Unalan, Thin films of hard cubic Zr_3N_4 stabilized by stress, Nat. Mater. 4 (2005) 317-322.

[3] A. Zerr, N. Chigarev, R. Brenner, D.A. Dzivenko, V. Gusev, Elastic moduli of hard c-Zr_3N_4 from laser ultrasonic measurements, Phys. Status Solidi - Rapid Res. Lett. 4 (2010) 353-355.

[4] M.A. El Hakim, M.D. Abad, M.M. Abdelhameed, M.A. Shalaby, S.C. Veldhuis, Wear behavior of some cutting tool materials in hard turning of HSS, Tribol. Int. 44 (2011) 1174-1181.

[5] W.P. Jiang, A.P. Malshe, A novel cBN composite coating design and machine testing: A case study in turning, Surf. Coat. Technol. 206 (2011) 273-279.

[6] D.A. Dzivenko, A. Zerr, V.K. Bulatov, G. Miehe, J. Li, B. Thybusch, J. Brötz, H. Fueß, G. Brey, R. Riedel, High-pressure multianvil synthesis and structure refinement of oxygen-bearing cubic zirconium(IV) nitride., Adv. Mater. 19 (2007) 1869-1873.

[7] J. Li, D. Dzivenko, A. Zerr, C. Fasel, Y. Zhou, R. Riedel, Synthesis of nanocrystalline Zr_3N_4 and Hf_3N_4 powders from metal dialkylamides, Z. Anorg. Allg. Chem. 631 (2005) 1449-1455.

[8] P. Kroll, Hafnium nitride with thorium phosphide structure: Physical properties and an assessment of the Hf-N, Zr-N, and Ti-N phase diagrams at high pressures and temperatures, Phys. Rev. Lett. 90 (2003) 125501.

[9] A. Zerr, H. Eschnauer, E. Kny, Hard materials, in: B. Elvers (Ed.) Ullmann's Encyclopedia of Industrial Chemistry, Electronic Release, Wiley-VCH, Weinheim/Germany, 2012, pp. 1-21.

[10] H.T. Hall, Ultra-high-pressure, high-temperature apparatus: the "Belt", Rev. Sci. Instrum 31 (1960) 125-131.

[11] C.-M. Sung, Optimised cell design for high-pressure synthesis of diamond, High Temp. - High Press. 33 (2001) 489-501.

[12] J.C. Sung, The eastern wind of diamond synthesis, New Diamond Front. Carbon Technol. 13 (2003) 47-61.

[13] Y. Kanke, M. Akaishi, S. Yamaoka, T. Taniguchi, Heater cell for materials synthesis and crystal growth in the large volume high pressure apparatus at 10GPa, Rev. Sci. Instrum 73 (2002) 3268-3270.

[14] T. Taniguchi, M. Akaishi, Y. Kanke, S. Yamaoka, TiC-diamond composite disk-heater cell assembly to generate temperature of 2000 °C in a large-volume belt-type high-pressure apparatus at 10GPa, Rev. Sci. Instrum 75 (2004) 1959-1962.

[15] G.B. Fairbank, C.J. Humphreys, A. Kelly, C.N. Jones, Ultra-high temperature intermetallics for the third millennium, Intermetallics 8 (2000) 1091-1100.

[16] J.K. Stalick, R.M. Waterstrat, The zirconium-platinum phase diagram, J. Alloy. Compd. 430 (2007) 123-131.

[17] D. Ott, C.J. Raub, Combined reduction of oxides by carbon in presence of metals of platinum group - part 2., Metall 32 (1978) 140-144.

[18] M. Lerch, F. Krumeich, R. Hock, Diffusion controlled formation of beta type phases in the system ZrO_2-Zr_3N_4, Solid State Ion. 95 (1997) 87-93.

[19] J.C. Gilles, Preparation par reaction a l'etat solide et structures des oxynitrures de zirconium, Bull. Soc. Chim. Fr. (1962) 2118.

[20] M. Lerch, Phase relationships in the ZrO_2-Zr_3N_4 system, J. Mater. Sci. Lett. 17 (1998) 441-443.

[21] K.S. Mazdiyasni, C.T. Lynch, J.S. Smith, Preparation of ultra-high-purity submicron refractory oxides, J. Am. Ceram. Soc 48 (1965) 372-375.

[22] E.C. Subbarao, H.S. Maiti, K.K. Srivastava, Martensitic transformation in zirconia, Phys. Status Solidi A 21 (1974) 9-40.

[23] N. Claussen, R. Wagner, L.J. Gauckler, G. Petzow, Nitride-stabilized cubic zirconia, J. Am. Ceram. Soc 61 (1978) 369-370.

[24] J. Mukerji, Stabilization of cubic zirconia by aluminum nitride, J. Am. Ceram. Soc 72 (1989) 1567-1568.

[25] M. Lerch, Neue Anionendefizit-Materialien auf der Basis von ZrO_2: Synthese, Charakterisierung und Eigenschaften von ternären und quaternären Nitridoxiden des Zirconiums (Habilitationsschrift), Bayerischen Julius-Maximilians-Universität, Würzburg, Germany, 1997.

[26] M.A. Pimenta, G. Dresselhaus, M.S. Dresselhaus, L.G. Cancado, A. Jorio, R. Saito, Studying disorder in graphite-based systems by Raman spectroscopy, Phys. Chem. Chem. Phys. 9 (2007) 1276-1291.

[27] C.M. Phillippi, K.S. Mazdiyasni, Infrared and Raman spectra of zirconia polymorphs, J. Am. Ceram. Soc 54 (1971) 254-258.

[28] T. Locherer, Hochdruck-Hochtemperaturverhalten von Zirkonium- und Hafnium-Oxonitriden, Fachbereich Material- und Geowissenschaften, Technische Universität Darmstadt, Darmstadt, Germany, 2009, pp. 141.

[29] S. Steeb, J. Renner, Ermittlung der Struktur des Tantalsuboxydes TaO_z (Ta_2O) mittels Elektronenbeugung, J. Less-Common Met. 9 (1965) 181-189.

[30] G. Brauer, K.H. Zapp, Die Nitride des Tantals, Z. Anorg. Allg. Chem. 277 (1954) 129-139.

[31] A. Zerr, G. Miehe, J. W. Li, D. A. Dzivenko, V. K. Bulatov, H. Hofer, N. Bolfan-Casanova, M. Fialin, G. Brey, T. Watanabe and M. Yoshimura, Adv. Funct. Mater. 19 (2009) 2282-2288.

FIGURES

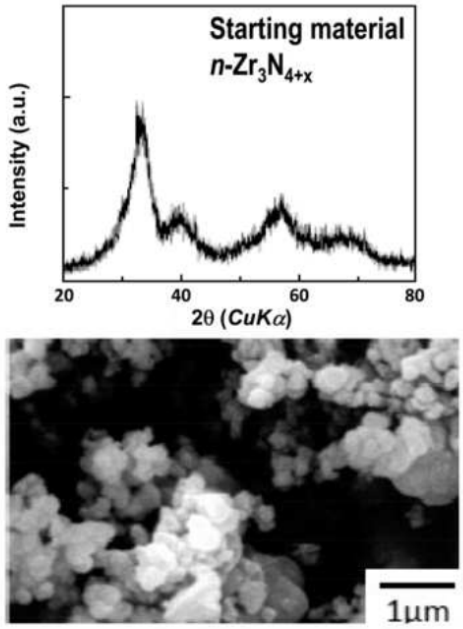

Fig. 1. XRD pattern and an SEM image of the starting n-Zr_3N_{4+x} powder.

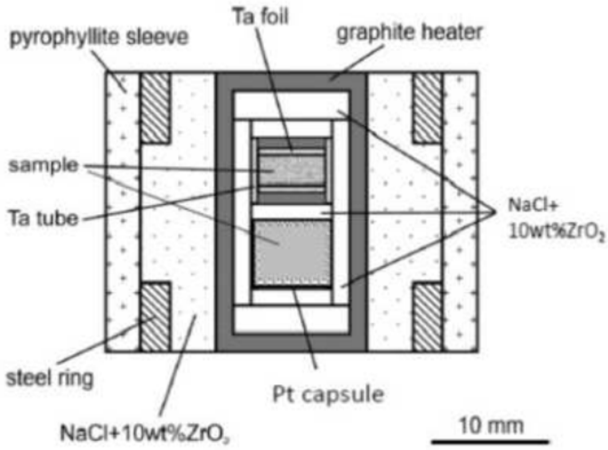

Fig. 2. Schematics of the sample assembly with two different capsules used in this work to synthesise c-Zr_3N_4 in the belt-type HP-HT apparatus.

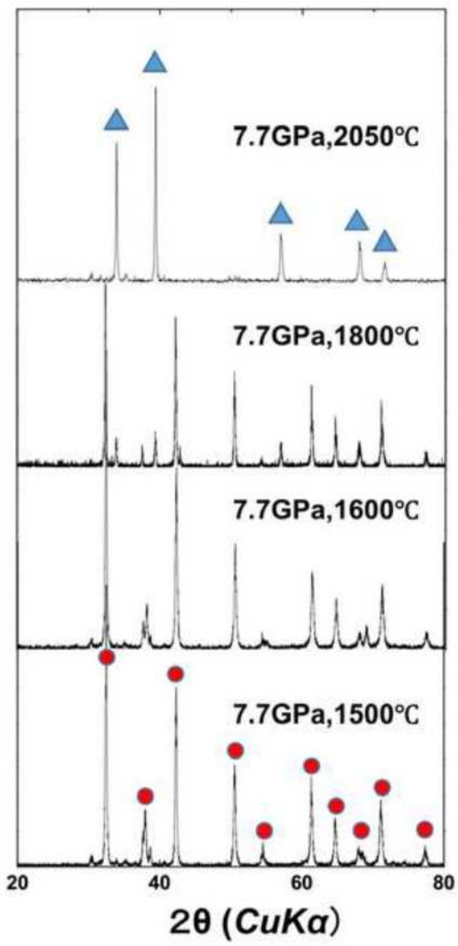

Fig. 3. XRD patterns of the products recovered after heating of the *n*-Zr_3N_{4+x} starting material at *P*=7.7 GPa to the indicated temperatures. Circles and triangles depict XRD peaks of c-Zr_3N_4 and ZrN, respectively.

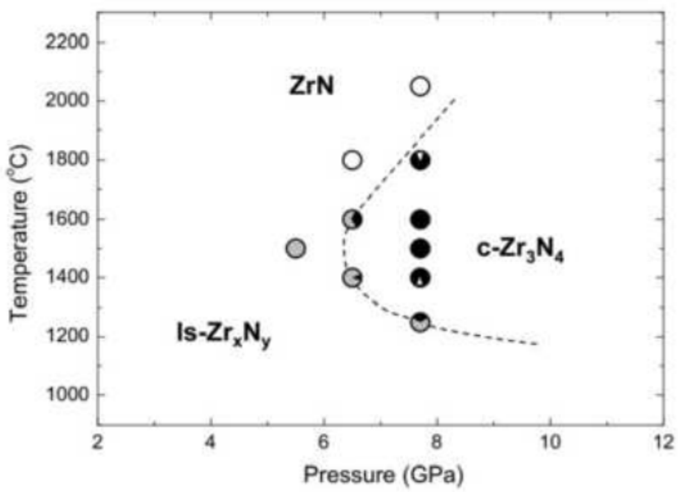

Fig. 4. *P-T* conditions of our synthesis experiments performed in the belt-type apparatus. Black, gray and white symbol colours represent the main compounds found in the recovered products, which were, respectively, c-Zr_3N_4, the low-symmetry zirconium nitride (ls-Zr_xN_y), and the mononitride ZrN. Segment sizes show qualitatively amounts of the corresponding compounds in the products. The dashed line is a guide for the eyes depicting the most probable boundary of the *P-T* region where c-Zr_3N_4 forms in a belt-type apparatus.

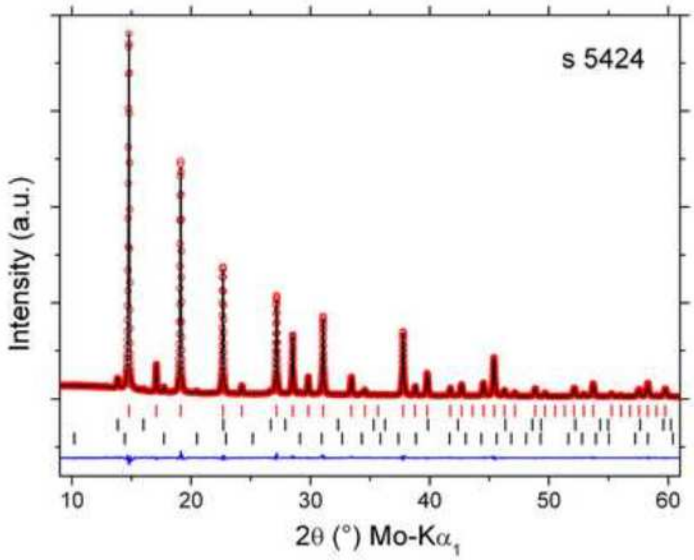

Fig. 5. XRD pattern (red open circles) of the product synthesised in a Pt capsule at *P*=7.7 GPa and *t*=1500 ºC. Result of the Rietveld refinement is shown by solid (black) line. The upper (red), middle, and lower tick marks show positions of the diffraction peaks of c-Zr_3N_4, c-ZrO_2, and the Pt-Zr based alloy, respectively. The bottom line (blue) represents the difference between the measured and the calculated XRD patterns. For c-Zr_3N_4, we obtained from the refinement R_{Bragg} = 1.4% and for the Zr-O rich by-product $R_{\mathrm{Bragg}} \leq 6.5\%$.

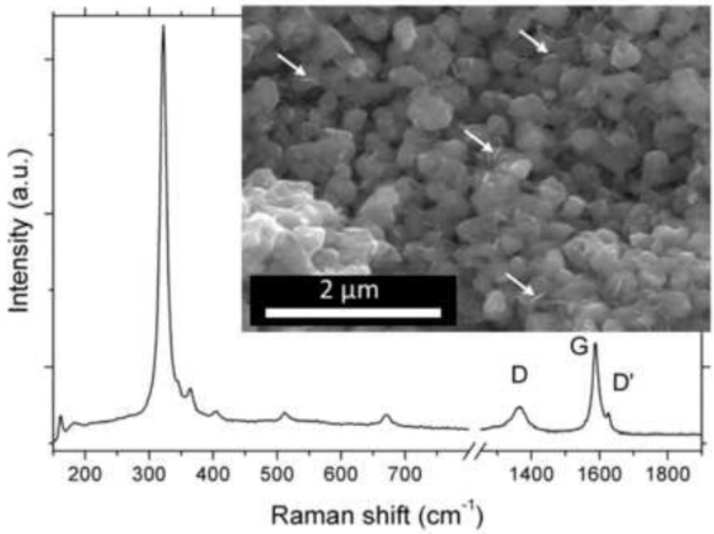

Fig. 6. Raman spectrum and an SEM image (inset) of the same sample as in Fig. 5. In addition to Raman bands of c-Zr_3N_4, the *D*-, *G*-, and *D´*-bands of disordered graphite were detected. The SEM image shows, in addition to grains of c-Zr_3N_4 of regular shapes and size typically <300 nm, thin platelets (some of them are indicated by arrows) of disordered graphite with the lateral dimensions around 150 nm and thickness of ~20 nm.

Table 1

Results of the elemental analysis (EA) based on the HGE measurements and of the phase analysis (PA) based on the XRD measurements of the starting material and of the HP-HT products (in wt%).

Starting	HP-HT products							
n-Zr_3N_{4+x}	s 5424				s 5006			
EA	EA	PA[a]			EA	PA[b]		
		Model 1						
N: 18.0(5)	N: 16.6(5)	c-Zr_3N_4 :	95.0(2)		N: 13.4(8)	c-$(Zr_{0.84}Ta_{0.16})_3N_4$:	93.9(3)	
O: 0.6(1)	O: 1.4(1)	c-ZrO_2 :	3.0(1)		O: 0.9(1)	c-ZrO_2 :	3.5(1)	
C: 1.4(1)	C: 1.6(1)	Pt_4Zr :	0.5(1)		C: 1.1(1)	Ta_2O :	1.2(1)	
						$TaN_{0.5}$:	0.3(1)	
		Model 2						
		c-Zr_3N_4 :	94.4(2)					
		$Zr_7O_8N_4$:	3.6(1)					
		Pt_4Zr :	0.5(1)					

[a] 1.5 wt% of disordered carbon were taken into account. [b] 1.1 wt% of disordered carbon were taken into account.